Structural Characterization and Electrochemical Reactions with Lithium of $Cu_2CoTi_xSn_{3-x}S_8$ Solid Solutions

P. Lavela, C. Pérez-Vicente, and J. L. Tirado*

Laboratorio de Química Inorgánica, Facultad de Ciencias, Universidad de Córdoba, Avda San Alberto Magno s/n, 14004, Córdoba, Spain

C. Branci, J. Olivier-Fourcade, and J. C. Jumas

Laboratoire de Physicochimie de la Matière Condensée (UMR 5617 CNRS), Université Monpellier II, Place Eugène Bataillon, 34095 Montpellier Cedex 5, France

Received January 4, 1999. Revised Manuscript Received June 10, 1999

The synthesis, structural determination, and electrochemical studies of $Cu_2CoTi_xSn_{3-x}S_8$ solid solutions are reported. The evolution of the cubic spinel unit cell parameter with x shows two regions which are defined by the increasing covalency of the Ti−S bonds and the radii of the metal ions present in the solid. An increase in the isomer shift of the ^{119}Sn Mössbauer spectra of these solids agrees with this interpretation. The solid solutions are used as active cathode materials in lithium cells. The discharge shows a complex reduction effect which is associated with the decrease in the oxidation state of Sn^{4+} and Ti^{4+} ions, accompanied by deep structural changes which end in the complete amorphization of the solid and the occurrence of tin in the metallic state. The extended discharge of the lithium cells leads to a good cycling behavior in galvanostatic experiments carried out in the 0−2.3 V interval, with capacities close to 400 mAh/g after 10 cycles.

Introduction

Tin and titanium chalcogenides provide numerous examples of interesting materials for advanced electrochemical systems. Both elements behave as active redox centers during the electrochemical insertion of lithium into different solids, which are useful electrode materials in lithium and lithium ion cells. The known host solids containing either the group 4 or group 14 elements that show good lithium insertion properties possess a wide structural diversity, having in common the presence of a large number of interconnected empty sites available for the diffusion and location of lithium ions. They span from layered solids, such as the 1T-binary dichalcogenides TiS_2[1−5] and SnS_2[6−9] to strictly three-dimensional lattices. The latter are represented by spinel-related solids, which include the cation-deficient tin-containing thiospinels $In_{16}Sn_4S_{32}$,[10,11] and rhodostannite-type $Cu_{3.31}GeFe_4Sn_{12}S_{32}$,[12] as well as the titanium compound $Cu_xTi_2S_4$.[13−16]

Among the quaternary tin-containing spinel systems, the solids with $Cu_{2-x}MSn_3S_8$ (M: Mn, Fe, Co, Ni) stoichiometry have provided interesting insertion behavior. The electrode performance in lithium anode cells is enhanced, particularly for the cobalt compound, by the previous extraction of copper from the tetrahedral sites in the structure. This can be achieved by using I_2−CH_3CN solutions as the oxidation reagent.[13,17] The resulting chemically Cu-deintercalated products have been used as active electrode material in lithium ion batteries vs $LiCoO_2$ cathodes.[18] Such cells provide a moderate capacity and a good cycling behavior in the 1−2 V potential range. Similarly, a good reversibility has been reported for $Cu_{0.18}Ti_2S_4$ when using a smooth lithium intercalation and deintercalation in lithium anode cells.[16]

With the aim of extracting the best of each element—tin and titanium, the synthesis, structural determination, and electrochemical studies of $Cu_2CoTi_xSn_{3-x}S_8$ solid solutions are reported here. From a electrochemical point of view, the interest of this substitution is to decrease the molecular weight and so to increase the

(1) Whittingham, M. S. *Prog. Solid State Chem.* **1978**, *12*, 41.
(2) Thompson, A. H. *J. Electrochem. Soc.* **1979**, *126*, 608.
(3) Schöllhorn, R. *Angew. Chem., Int. Ed. Engl.* **1980**, *19*, 983.
(4) Dahn, J. R.; Haering, R. R. *Solid State Commun.* **1981**, *40*, 245.
(5) Eisenberg, M. *Electrochim. Acta* **1981**, *26*, 955.
(6) Danot, M.; LeBlanc, A.; Rouxel, J. *Bull. Soc. Chim. Fr.* **1969**, *8*, 2670.
(7) Morales, J.; Perez-Vicente, C.; Tirado, J. L. *Solid State Ionics* **1992**, *51*, 133.
(8) Pietrass, T.; Taulelle, F.; Lavela, P.; Olivier-Fourcade, J.; Jumas, J. C.; Steuernagel, S. *J. Phys. Chem. B* **1997**, *101*, 6715.
(9) Morales, J.; Perez-Vicente, C.; Santos, J.; Tirado, J. L. *J. Electrochem. Soc.* **1996**, *143*, 2847.
(10) Morales, J.; Tirado, J. L.; Elidrissi-Moubtassim, M. L.; Olivier-Fourcade, J.; Jumas, J. C. *J. Alloy Compd.* **1995**, *217*, 176.
(11) Elidrissi-Moubtassim, M. L.; Bousquet, C.; Olivier-Fourcade, J.; Jumas, J. C.; Tirado, J. L. *Chem. Mater.* **1998**, *10*, 968.
(12) Bousquet, C.; Perez-Vicente, C.; Krämer, A.; Tirado, J. L.; Olivier-Fourcade, J.; Jumas, J. C. *J. Mater. Chem.* **1988**, *8*, 1399.
(13) Schöllhorn, R.; Payer, A. *Angew Chem.* **1985**, *97*, 57.
(14) James, A. C. W. P.; Goodenough, J. B.; Clayden, N. J.; Banks, P. M. *Mater. Res. Bull.* **1989**, *24*, 143.
(15) Jacobsen, T.; Zachau-Christiansen, B.; West, K.; Atlung, S. *Electrochim. Acta* **1989**, *34*, 1473.
(16) Imanishi, N.; Inoue, N.; Takeda, Y.; Yamamoto, O. *J. Power Sources* **1993**, *43*−*44*, 619.
(17) Lavela, P.; Tirado, J. L.; Morales, J.; Olivier-Fourcade, J.; Jumas J. C. *J. Mater. Chem.* **1996**, *6*, 41.
(18) Cochez, M. A.; Jumas, J. C.; Lavela, P.; Morales, J.; Olivier-Fourcade, J.; Tirado, J. L. *J. Power Sources* **1996**, *62*, 101.

10.1021/cm990003e CCC: $18.00
Published on Web 10/01/1999

specific capacity. In some cases, it also allows the improvement of the electrical conductivity[19] and insertion properties as anodic materials. X-ray diffraction (Rietveld method), Mössbauer spectrometry, and some crystallographic calculations have been done to carry out this structural characterization. In the study of the electrochemical lithium intercalation into these multielement systems, Step Potential Electrochemical Spectroscopy (SPES) is used here. According to Chabre,[20] this technique can be considered as a combination of the Potential Intermittent Titration Technique (PITT)[21] and the electrochemical potential spectroscopy.[2] It can provide a valuable tool for the study of the different steps that may be present in the reduction−oxidation reactions. In fact, it has been successfully applied to the study of systems with structural complexity, such as C_{60} [22] and MTe_2 (M: V, Nb, Ta).[23, 24]

Experimental Section

All samples were prepared from stoichiometric powder mixtures of the pure elements, placed in evacuated silica tubes ($P < 10^{-3}$ Pa) and sealed. These mixtures were heated to 300 °C for 1 day. The temperature was then increased to achieve a final constant value of 750 °C for 10 days. The product compounds were obtained as black powders, which were ground and stored under vacuum to avoid oxidation or hydrolysis.

X-ray powder diffraction patterns (XDP) were alternatively recorded on a PHILIPS and a SIEMENS D5000 diffractometer using Cu Kα radiation. For analyzing the structural modifications induced by the different cation substitution, Rietveld analyses of XDP were carried out, with the aid of the computer program *Rietveld Analysis Program DBWS-9411*.[25]

Mössbauer spectra were recorded at room temperature in the constant-acceleration mode on a ELSCINT-AME40. The γ-ray source was $Ba^{119m}SnO_3$ and the velocity scale was calibrated with the magnetic sextet spectrum of a high-purity iron foil absorber, using ^{57}Co(Rh) as source. Recorded spectra were fitted to Lorentzian profiles by least-squares method with the computer program ISO,[26] and the fit quality was controlled by the classical χ^2. The origin of the isomer shifts was determined from the center of the $BaSnO_3$.

The electrochemical lithium insertion was carried out in two-electrode cells Swagelock type. The electrolyte was a 1 M solution of $LiClO_4$ in propylenecarbonate (PC), supported in a glass-paper disk (Whatman Glass Microfiber).

For the step potential electrochemical spectroscopy (SPES) experiments, the cathode was prepared from the pure compound. The pellets of 7 mm diameter were obtained by pressing 20−30 mg of powder sample at 1.5 tons/cm^2. The anode was a metallic lithium disk. The discharge curve was obtained at room temperature by using a multichannel microprocessor-controlled system (MacPile). An initial relaxation was allowed until $\Delta V/\Delta t$ was lower than 1 mV/h. The voltage steps during the discharge were fixed to 10 mV during 1 h or until the current passing through the cell was lower than 0.2 μA. The average lithium content was calculated from the amount of electron charge transferred to the cathode, on the assumption that no current was due to side reactions.

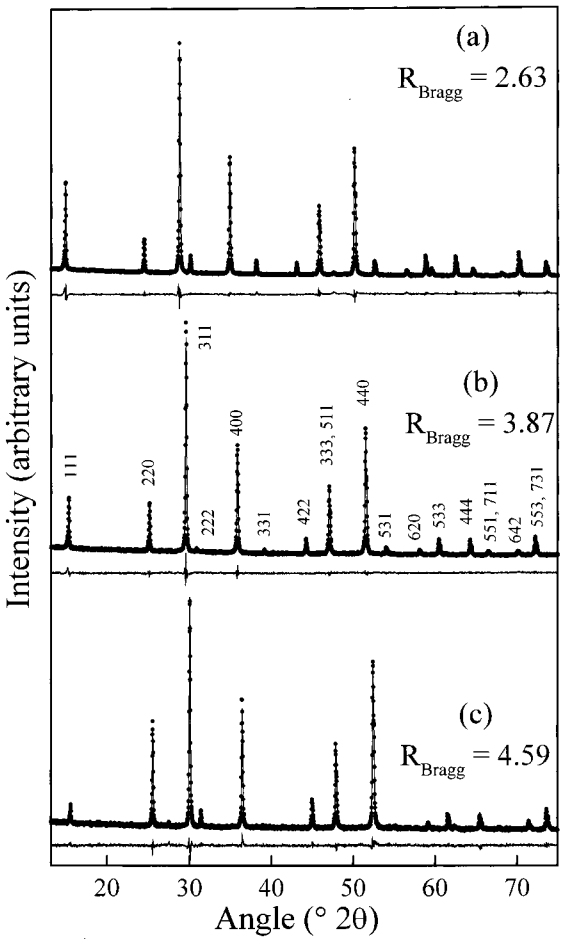

Figure 1. Experimental (dots), calculated (solid line), and difference (below) X-ray diffraction patterns of solid solutions with nominal compositions: (a) $Cu_2CoSn_3S_8$, (b) $Cu_2CoTi_{1.5}Sn_{1.5}S_8$, and (c) $Cu_2CoTi_3S_8$.

The galvanostatic cycling experiments were carried out in a computer-controlled AMEL 1480 galvanostat. The 7-mm-diameter cathode pellets now consisted of 80% host material (2.1−2.7 mg), 10% carbon black, and 10% PTFE binder, pressed on a steel grid at 1.5 tons/cm^2. The cell currents were in the 22−25 μA range (57−65 μA cm^{-2} current densities) to reach 1F/mol each 4 h.

Results and Discussion

Structural Characterization by X-ray Diffraction. X-ray powder diffraction patterns (XDP) of all compounds showed that the reaction of the starting elements was completed within the selected reaction time. The XDP were indexed according to a cubic spinel-related structure ($Fd\bar{3}m$ space group) and refined by Rietveld analysis. The results of this refinement confirmed the spinel structure of all solids with M and Ti/Sn atoms placed in the octahedral 16d site, while Cu atoms are located in the tetrahedral 8a site. The Ti/Sn substitution was shown to be topotatic in the 16d site, while the distribution of the other cations within the spinel framework remained unchanged. Because of the similarity of the patterns obtained for the set of compounds studied here, we only present some selected patterns of the $Cu_2CoTi_xSn_{3-x}S_8$ series in Figure 1. The Sn/Ti substitution induces significant changes in the relative intensity of some reflections. Thus, the intensity of the (111) reflection is dependent on the relative scattering factor of atoms located in octahedral vs

(19) Branci, C.; Sarradin, J.; Olivier-Fourcade, J.; Jumas, J. C. *Mol. Cryst. Liq. Cryst.* **1998**, *311*, 69.
(20) Chabre, Y. *J. Electrochem. Soc.* **1991**, *138*, 329.
(21) Weppner, W.; Huggins, R. A. *Annu. Rev. Mater. Sci.* **1978**, *8*, 269.
(22) Chabre, Y.; Djurado, D.; Armand, M.; Romanow, W. R.; Coustel, N.; McCauley, J. P.; Fischer, J. E.; Smith, A. B. *J. Am. Chem. Soc.* **1992**, *114*, 764.
(23) Guzmán, R.; Morales, J.; Tirado, J. L. *J. Mater. Chem.* **1993**, *3*, 1271.
(24) Guzmán, R.; Morales, J.; Tirado, J. L. *Chem. Mater.* **1995**, *7*, 1171.
(25) Young, R. A.; Sakthivel, A.; Moss, T. S.; Paiva-Santos, C. O. *J. Appl. Crystallogr.* **1995**, *28*, 366.
(26) Kundig, W. *Nucl. Instr. Methods* **1979**, *75*, 336.

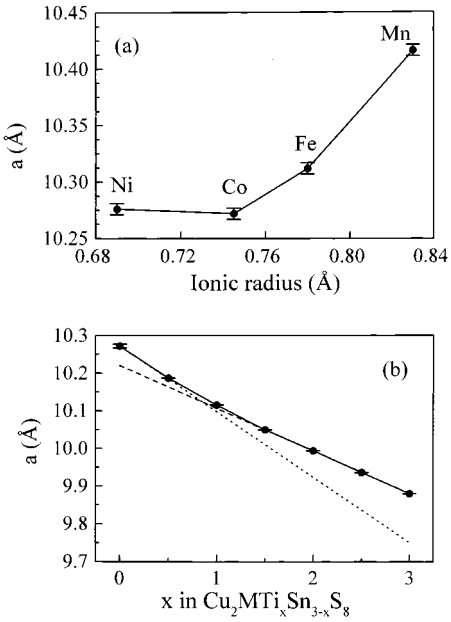

Figure 2. Evolution of the cubic-spinel lattice parameter *a* with (a) ionic radii of high-spin M^{2+} ions in $Cu_2CoMSn_3S_8$ solid solutions (M = Mn, Fe, Co, and Ni) and (b) *x* in $Cu_2CoTi_xSn_{3-x}S_8$.

tetrahedral sites. The Sn/Ti substitution leads to a decrease of the scattering factor in octahedral sites, thus leading to a decrease in the (111) line intensity. Concerning the (220) reflection, the effect is the opposite to that previously described and a net increase of intensity is observed. In contrast, for the different M atoms (Mn, Fe, Co, Ni), no important variation in intensity is observed due to the similar scattering factors of the different M atoms.

Effects of Ionic Radius. *a. $Cu_2MSn_3S_8$ (M = Mn, Fe, Co, Ni) System.* Figure 2a shows the evolution of the unit cell parameter *a* as a function of the ionic radii of the M^{2+} cations, r_M, according to the data published by Shannon[27] for octahedrally coordinated ions in a high-spin configuration. A decrease in both *a* and r_M parameters is observed from Mn to Co, while no additional decrease in *a* exists from Co to Ni, although Ni^{2+} has the lowest r_M. As Sn^{4+} together with Ni^{2+} have a lower size than the other M^{2+} ions, the main origin of the possible expansion of the framework can be ascribed to the size of the M^{2+} cations. Thus, the cation/sulfur anion radii ratio (r_M/r_S) can be calculated by using the value of effective ionic radii obtained for S^{2-} by the systematic study of the interatomic distances in chalcogenides reported by Shannon[27] (1.84 Å). If the calculated ratios are compared to the theoretical maximum value for a close-packet arrangement, 0.4142, the obtained values show that the size of the octahedral site can accommodate Co^{2+} and Ni^{2+} (r_M/r_S = 0.4049 and 0.3750, respectively), but this is not the case for Mn^{2+} and Fe^{2+} (r_M/r_S = 0.4511 and 0.4239, respectively) ions. Thus, S^{2-} atoms have to be taken away from each other to increase the size of the octahedral site and allow Mn^{2+} and Fe^{2+} ions to be accommodated in this site.

It is well-known that the efficiency in the use of space in solids structurally derived from a closest packing of rigid spheres (S) may show three well-defined regions of r_M/r_S ratio: M−M, M−S, and S−S contacts.[28] For octahedral site occupancy, cations with r_M/r_S ratio lower than 0.4142 are in the S−S contacts region while larger values imply M−S contacts. The unit cell parameter in the former region is not dependent on the size of M while the opposite is true for the M−S region. Thus, no changes of *a* with r_M are expected from Co^{2+} to Ni^{2+}, which agrees fairly well with the plot in Figure 2a.

b. Substitution Ti/Sn: $Cu_2CoTi_xSn_{3-x}S_8$ System. Figure 2b shows the evolution of the unit cell parameter as a function of the titanium content for M = Co. A decrease in *a* is observed on increasing the titanium content. This sequence could be explained by the lower ionic radius of titanium as compared with tin ions. However, the Sn/Ti size effect alone is not sufficient to explain the observed changes, as the octahedral Co^{2+} ions have a larger size than either Sn^{4+} or Ti^{4+} ions. Thus, the changes in the unit cell dimensions are impeded by preserving M−S contacts. Alternatively, it should be noted that the lower size of Ti^{4+} as compared with Sn^{4+} implies a higher polarization of the anions and a more covalent character of the bonds formed with sulfur atoms. This effect is discussed below on the light of the Mössbauer data. The increasing covalent character in turn, leads to the decrease of the effective size of the S^{2-} anion and the unit cell dimensions.

From a more detailed inspection of Figure 2b, it can be observed that the slope of the curve is not constant in the complete composition interval. On the contrary, two regions are discernible. To understand this complex behavior, the effective size of the S^{2-} anions should be known at each composition in order to estimate the spinel unit cell parameter. This is a difficult task as it is not possible to find an equivalent set of compounds. However, the experimental values can be compared with those found in related compounds having only Ti^{4+} or Sn^{4+} octahedrally coordinated by sulfide anions. For Ti^{4+} sulfides two different systems can be used: spinel type Ti_2S_4 and layered 1T-TiS_2. The former compound is not know, although compounds in the $Cu_{1-x}[Ti_2]S_4$ series have been obtained by chemical deintercalation of copper up to $x = 0.93$.[14] A linear contraction of the lattice was found as the copper is extracted. The extrapolated value for $x = 1$ is then ~9.75 Å. This value is slightly lower than that obtained for $Cu_2CoTi_3S_8$ (9.85 Å). Unfortunately, a similar compound containing Sn^{4+} only is not known. Alternative values can be derived from the unit cell parameter *a* of trigonal TiS_2 and the isostructural compound SnS_2.[29] The values obtained assuming S−S contacts within the layers of the disulfides were $r_{S(Ti)}$ = 0.8515 Å and $r_{S(Sn)}$ = 0.9105 Å, respectively. These values can be converted to a hypothetical cubic-spinel unit-cell parameter by simple multiplying by the $8\sqrt{2}$ factor. The cubic *a* values obtained for "$[Ti_2]S_4$" and "$[Sn_2]S_4$" by this procedure are 9.634 and 10.301 Å, respectively. While the latter value is close to that obtained for $Cu_2CoSn_3S_8$ (10.272 Å), the value for the titanium compound differs more markedly from the value extrapolated from the isostructural spinels $Cu_{1-x}[Ti_2]S_4$. For intermediate Ti/Sn

(27) Shannon, R. D. *Acta Crystallogr.* **1976**, *A32*, 751.

(28) Parthé, E. *Z. Kristallogr.* **1961**, *115*, 52.

(29) Bachin, A. A. In *Crystallography and crystal Chemistry of Materials with Layered Structure*; Lévy, F., Ed.; Reidel: Dordrecht, 1976.

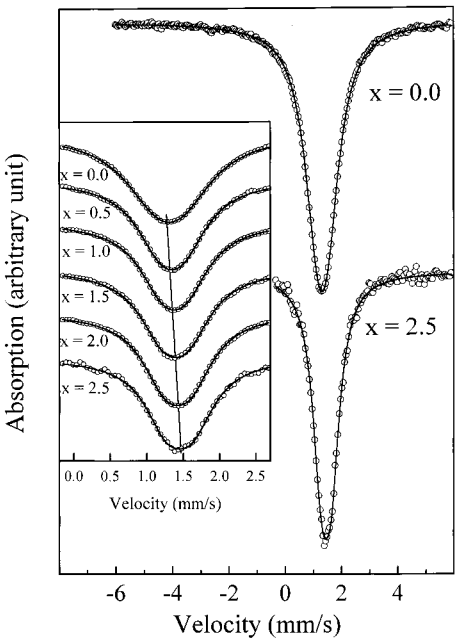

Figure 3. Experimental (circles) and calculated (solid lines) ^{119}Sn Mössbauer spectra of $Cu_2CoTi_xSn_{3-x}S_8$ solid solutions for $x = 0$ and 2.5. Inset: detail in the 0−2.5 mm/s velocity range for different x values.

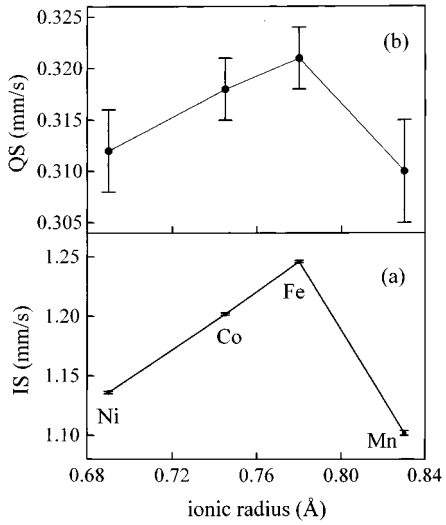

Figure 4. Changes in (a) isomer shift (IS) and (b) quadrupole splitting (QS) derived from ^{119}Sn Mössbauer spectra vs ionic radii of high-spin M^{2+} ions in $Cu_2CoMSn_3S_8$ solid solutions (M = Mn, Fe, Co, and Ni).

Table 1. Isomer Shift (IS), Quadrupole Splitting (QS), and Line Width at Half Maximum (LW) Derived from the ^{119}Sn Mössbauer Spectra of $Cu_2CoTi_xSn_{3-x}S_8$ Solid Solutions

x in $Cu_2CoTi_xSn_{3-x}S_8$	IS (mm/s)	QS (mm/s)	LW (mm/s)
0.0	1.202(1)	0.318(6)	0.863(6)
0.5	1.247(4)	0.314(8)	0.839(8)
1.0	1.281(3)	0.320(5)	0.823(5)
1.5	1.297(3)	0.342(6)	0.811(7)
2.0	1.327(2)	0.350(4)	0.786(5)
2.5	1.354(6)	0.353(10)	0.755(13)

compositions, the unit cell dimensions have been interpolated from the best estimates (extrapolated Ti_2S_4 and layered SnS_2) and are plotted in Figure 2b. It can be seen that the sequence is only followed by tin-rich compositions up to $x = 1.0$, which can be considered an intermediate situation between two different sequences.

The sequence in the second part of the plot (for $x =$ 1.5 to 3) should take into account the size of Co^{2+} ions, as the effective ionic radii reported for Ti^{4+}, 0.605 Å,[27] is clearly lower than that for Co^{2+}. Thus, we can expect that Co^{2+} is the cation that determines the extent in which further contraction of the spinel cell takes place after the average Sn/Ti size has been reduced by substitution values $x > 1$.

^{119}Sn Mössbauer and XAS Studies. To obtain complementary information about the local environment of tin atoms in these thiospinels, ^{119}Sn Mössbauer spectra were recorded. Irrespective of the nature of M in $Cu_2MSn_3S_8$, the spectra are characterized by the presence of a single signal, with a quadrupolar splitting, which is not clearly resolved from a visual inspection of the spectrum, as shown for M = Co in Figure 3 ($x =$ 0 in $Cu_2CoTi_xSn_{3-x}S_8$). The isomer shift (IS) values were in the 1.1−1.2 mm/s range for all compositions (Figure 4a), which is characteristic of Sn^{4+} in octahedral coordination. The quadrupolar splitting parameter (QS) could be calculated from the fitting of the profile to two Lorentzian lines. The values obtained by this procedure are low but significant (up to ∼0.32 mm/s, Figure 4b), thus being indicative of a slightly distorted octahedral environment of tin atoms. The existence of a quadrupole split signal is explained by an electric field gradient resulting from a trigonal field of the six nearest S atoms, which are not in a perfect octahedral symmetry. This distortion is originated by the random distribution of Sn^{4+} and M^{2+} cations in the second neighbor octahedral sites. Figure 4a represents the evolution of IS as a function of the Shannon[27] ionic radii of the transition element cations M^{2+}. We can observe a decrease from Fe to Co and Ni. This is the expected sequence if we take into account the evolution in the size of the divalent ions. On decreasing size, M^{2+} ions possess a stronger polarizing power, thus inducing an increase of the covalency in Ni−S bonds. In consequence, the covalent character of the Sn−S bonds decreases accordingly and a decrease in the value of IS is observed. However, the IS value obtained for Mn, with the largest ionic radius is lower than those observed for the iron or even the nickel compound. The interpretation of this apparent discrepancy should take into account the evolution of QS. From a comparison of parts a and b of Figure 4, it is clear that a correlation effect between QS and IS values is observed. The larger QS values of Co and Fe compounds can be related with the enhanced anisotropy of the electric field for the high-spin octahedral ions Co^{2+} ($t_{2g}^5e_g^2$) and Fe^{2+} ($t_{2g}^4e_g^2$), as compared with Ni^{2+} ($t_{2g}^6e_g^2$) and Mn^{2+} ($t_{2g}^3e_g^2$). These differences lead to a larger electric field around the Sn^{4+} ions which have cobalt and iron ions as second neighbors. Moreover, the spherical field around nickel and manganese ions make ionicity of the Sn−S bond higher, and thus decrease the IS values.

Concerning the $Cu_2CoTi_xSn_{3-x}S_8$ series, the hyperfine parameters obtained by ^{119}Sn Mössbauer spectroscopy (Figure 3) are included in Table 1. These data confirm that tin atoms remain in Sn(IV) formal oxidation state in a very slightly distorted octahedral environment (low values of QS). The Sn/Ti substitution is accompanied

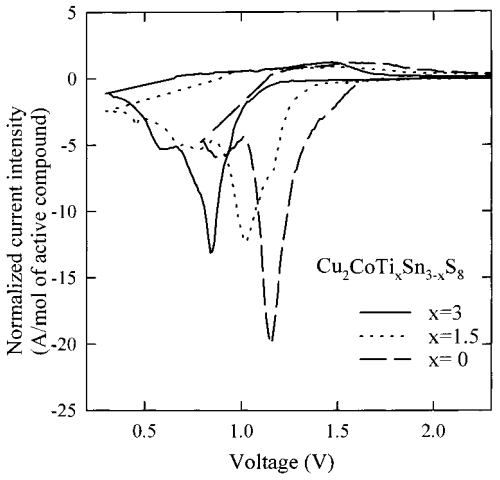

Figure 5. Normalized current intensity versus voltage curves obtained by SPES of lithium cells using $Cu_2CoTi_xSn_{3-x}S_8$ (x = 0, 1.5, and 3.0) as cathode material.

by an increase of the isomer shift. We can note the existence of two simultaneous effects:

First, Ti(IV) has a stronger polarizing power as compared to Sn(IV), leading to an increase of the covalency of Ti−S bonds, and so to a decrease of the covalent character of Sn−S bonds with a decrease of the isomer shift.

Second, a decrease of the distance between atoms in Sn−S bonds reveals an increase of the covalent character of bonds. IS is directly proportional to the electronic density at the core, and the IS increases during the Sn/Ti substitution process. Table 1 illustrates the evolution of IS when compared with the unit cell parameters in Figure 2b.

It is difficult to evaluate the weight of each factor and isolate them, but in the light of the experimental data it seems evident than the second effect is more important than the first one, leading to an increase of IS after Sn/Ti substitution.

As additional characterization of the local environment of Sn, Ti, Fe, and S atoms present in these thiospinels, X-ray absorption measurements were carried out. The absorption spectra were compared to those of the binary compounds SnS_2, TiS_2, and FeS, allowing a simple attribution of the electronic transition observed in the thiospinel compounds. Thus, for example, from the study at the S−K edge, it can be concluded that the (Sn 5s (or Ti $3d_{t2g}$) − S 3p)* and (Sn 5p (or Ti $3d_{eg}$) − S 3p)* overlapping mainly constitutes the first empty states with a S 3p character. This study also concludes that the local environments of Ti, Sn, Fe, and Co remain unchanged during the substitution of Sn by Ti. A detailed analysis of these results will early be published separately.[30]

Electrochemical Reactions of $Cu_2CoTi_xSn_{3-x}S_8$ Solid Solutions with Lithium. Step potential electrochemical spectroscopy (SPES) was chosen as the main technique to study the electrochemical behavior of the spinel electrode materials during the first steps of the discharge of lithium cells. The normalized current intensity versus voltage curves for $Cu_2CoTi_xSn_{3-x}S_8$ for x = 0, 1.5 and 3.0 are shown in Figure 5. The main

(30) Branci, C.; Womes, M.; Lippens, P. E.; Olivier-Fourcade, J.; Jumas, J. C. *J. Mater Chem.* 1988. Submitted for publication.

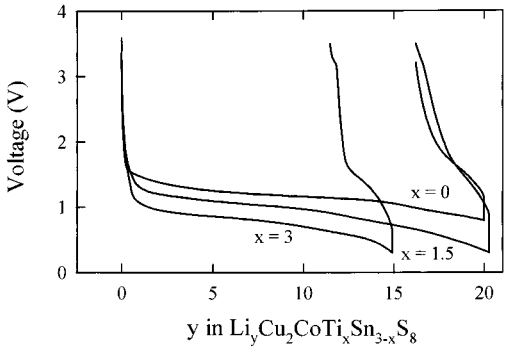

Figure 6. Cell voltage vs depth of discharge obtained by SPES of lithium cells using $Cu_2CoTi_xSn_{3-x}S_8$ (x = 0, 1.5, and 3.0) as cathode material.

reduction peak occurs at cell voltage values which decrease as tin atoms are replaced by titanium atoms. No splitting of the main signal was observed for the intermediate composition $Cu_2CoTi_{1.5}Sn_{1.5}S_8$ that could be ascribed to the separated reduction of tin and titanium atoms. Thus, the reduction of both elements can be considered to take place simultaneously, during the incorporation of lithium into the electrode material. It should be noted that the discharge curves of TiS_2 and SnS_2 show similar average cell potentials up to 1 F/mol, although the slope of V vs x is more marked in Li_yTiS_2 than in Li_ySnS_2.[2,7] These data are in apparent contradiction with the significant changes in peak voltage with Sn/Ti ratio which are observed in Figure 5. The observed changes are then ascribable to the different structures of the spinel chalcogenide parent material as compared with the layered dichalcogenides.

Attempts to cycle the lithium cells after the first reduction peak failed, as revealed in both Figure 5 and the corresponding voltage versus composition curves (Figure 6). Moreover, the low slope of the discharge profile may involve multiphase irreversible reactions. To assess for the origin of the lack of reversibility of the first step, intermediate lithiated samples with nominal composition "$Li_yCu_2CoTi_xSn_{3-x}S_8$" were prepared by interrupting the discharge experiments at different y values. The X-ray diffraction pattern of selected samples are shown in Figure 7. While little lattice expansion was detected on intercalation, changes in the relative intensities of the diffraction lines are detected for y = 1. These are particularly evident for 311/440 lines and can be qualitatively explained in terms of a cation redistribution which increases the scattering factor of octahedral sites 16c or 16d vs tetrahedral 8a sites. Nevertheless, it should be noted that changes in the coordinates of sulfur atoms may also affect the intensity ratios. Attempts to perform a Rietveld refinement of the patterns did not converge in acceptable R values and thus the results are not shown. Moreover, the continuous loss of line intensity observed in X-ray diffraction patterns in Figure 7 as lithium content increases makes evident a structural amorphization of the spinel phase. In addition, X-ray diffraction patterns make evident a reduction of copper. The lines corresponding to fcc copper are visible above 4 F/mol.

To study the reduction of tin atoms during cell discharge, room-temperature ^{119}Sn Mössbauer spectroscopy was used. Figure 8 shows the experimental and

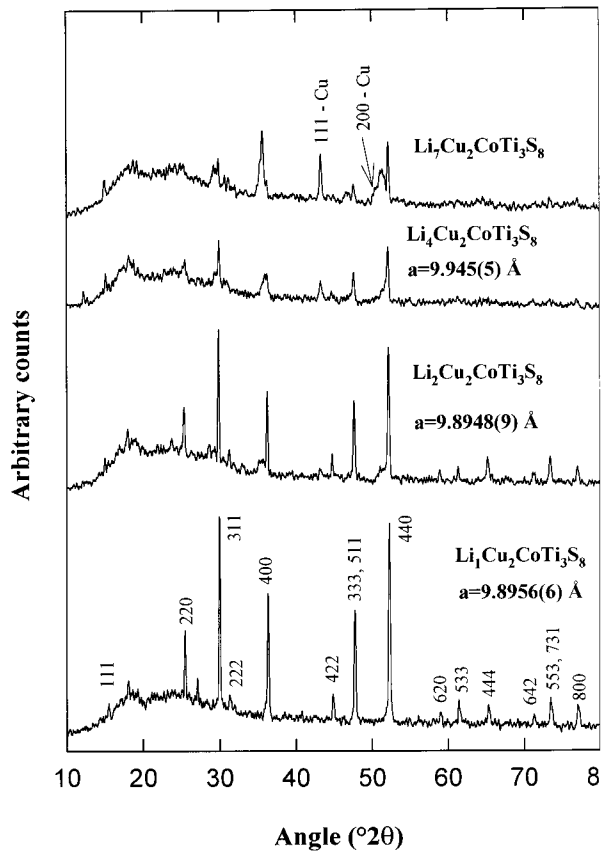

Figure 7. Powder X-ray diffraction patterns of lithiated intermediates obtained by interrupting the discharge experiments for Cu_2CoTiS_8.

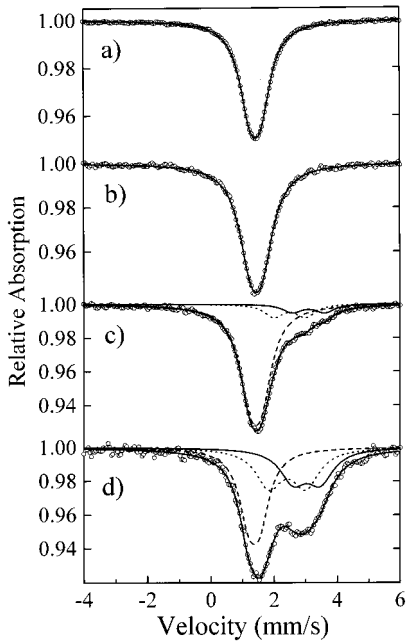

Figure 8. Experimental (circles) and calculated (lines) ^{119}Sn Mössbauer spectra of discharged electrodes with nominal compositions $Li_yCu_2CoTi_{1.5}Sn_{1.5}S_8$ for (a) $y = 0$, (b) $y = 2$, (c) $y = 4$, and (d) $y = 12$.

calculated spectra of discharged electrodes with nominal compositions $Li_yCu_2CoTi_{1.5}Sn_{1.5}S_8$ for $y = 0$, 2, 4, and 12. The hyperfine parameters are listed in Table 2. With regard to the lithiated samples, the reduction process can be divided in two steps. In the first step, below $y =$ 4, no additional subspectrum to the typical octahedral Sn^{4+} quadrupole signal described above is observed. In the second step, $y \geq 4$, two subspectra appear with isomer shifts corresponding to tin associated to a lower oxidation state (IS = 3 mm/s for the Sn^{2+} and IS = 2.3 mm/s for the Sn^0). These complex spectra imply the simultaneous reduction of Sn^{4+} to Sn^{2+} and Sn^0, as found in other tin sulfides such as SnS_2.[31] For $y = 12$, Sn^{4+} is not quantitatively reduced, since the signal at IS = 1.21 mm/s represents approximately 38% of total tin.

Table 2. Isomer Shift (IS), Quadrupole Splitting (QS), Line Width at Half Maximum (LW), and Relative Absorption (RA) Derived from the ^{119}Sn Mössbauer Spectra of $Li_xCu_2CoSn_{1.5}Ti_{1.5}S_8$

site	*x*	IS (mm/s)	QS(mm/s)	LW(mm/s)	RA (%)
Sn(IV)	0	1.327(1)	0.350(4)	0.786(5)	100
	2	1.341(3)	0.350(6)	0.922(6)	100
	4	1.332(9)	0.35(1)	0.85(1)	78
	12	1.215(9)	0.27(1)	0.80(1)	38
Sn(II)	4	3.01(9)	1.0(1)	0.96(8)	7
	12	2.99(7)	1.05(3)	0.97(5)	20
Sn(0)	4	2.39(4)	1.07(6)	0.96(8)	15
	12	2.296(7)	1.32(1)	0.97(5)	42

The importance of the structural changes described above is then related to the fact that insertion of large amounts of lithium destroys the spinel structure as well as leads to the occurrence of Sn^0. This in turn leads to a poor reversibility of the first discharge step (Figures 5 and 6). However, the reduction of tin and the presence of the metal as highly dispersed clusters in the noncrystalline sulfide matrix may allow further extension of the electrochemical process below 1 V.[33] At these lower voltages, the formation of lithium−tin alloys may take place. In fact, this is the basis of the recently claimed anode materials for lithium ion cells.[32]

Figure 9 shows the results obtained by the galvanostatic discharge of lithium cells to a voltage of 0 V followed by the first charge to 2.3 V for $Cu_2CoSn_3S_8$ and to 1.8 V for $Cu_2CoTi_3S_8$. The second discharge to 0 V for both compositions is also included. The less steep region leading to the peaks in Figure 5 is again visible below 500 mAh/g of active compound and is more clearly evidenced in the plots of incremental capacity, which are shown as insets in Figure 9. Some differences with the nominal voltage at which the reduction takes are observed between Figures 5 and 9 which are ascribable to the different methods of study (SPES and galvanostatic, respectively) and the departure from true equilibrium conditions. Nevertheless, the voltage sequence observed by SPES, i.e., higher voltage for the tin compound, is preserved.

After the main reduction effect, two new pseudoplateaus occur for the tin containing sample at ~0.9 and 0.2 V (Figure 9). The lower voltage effect has an extension of ~400 mAh/g of active cathode material and could be associated with tin−lithium alloying processes. In fact this effect is not observed for $Cu_2CoTi_3S_8$. Moreover, if we take into account the maximum alloying

(31) Olivier-Fourcade, J.; Jumas, J. C.; Womes, M.; Lavela, P.; Tirado, J. L.; Morales, J. *Conference Proceedings "ICAME/95"* **1996**, *50*, 75.

(32) Courtney, I. A.; Dahn J. R. *J. Electrochem. Soc.* **1997**, *144*, 2045.

(33) Courtney, I. A.; McKinnon W. R.; Dahn, J. R. *J. Electrochem. Soc.* **1999**, *146*, 59.

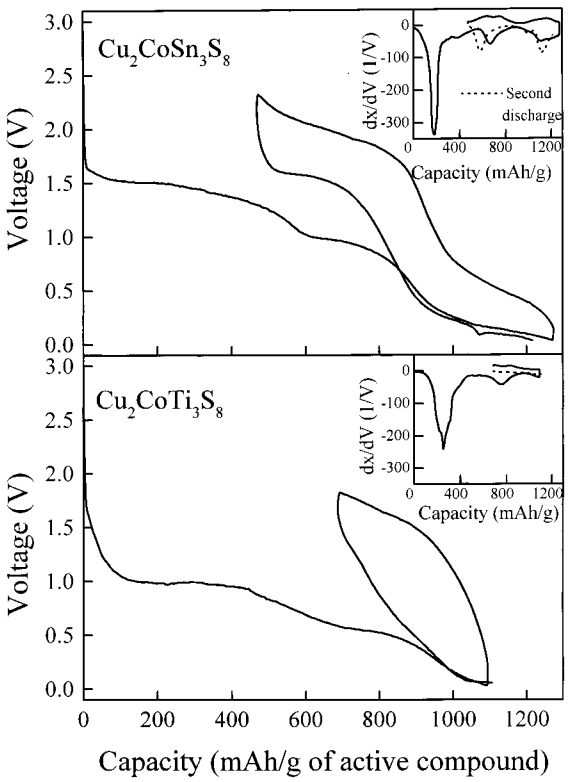

Figure 9. Galvanostatic discharge−charge−discharge cycle of lithium cells using $Cu_2CoTi_xSn_{3-x}S_8$ (x = 0 and 3.0) as cathode material. The plot of the dx/dV derivative vs capacity are shown as insets.

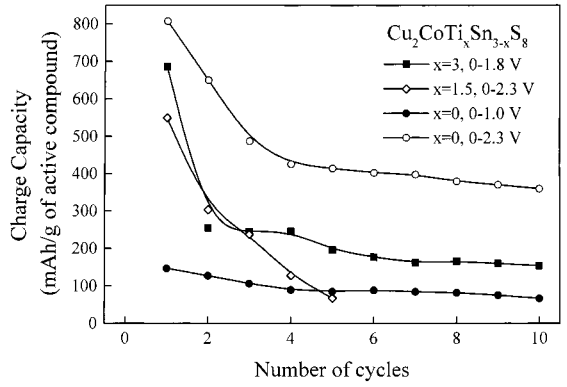

Figure 10. Plots of cell capacity vs cycle number for lithium cells using $Cu_2CoTi_xSn_{3-x}S_8$ (x = 0, 1.5, and 3.0) as cathode material and cycled under galvanostatic conditions.

capacity of tin metal (up to $Li_{4.4}Sn$[33]), this gives a maximum reversible capacity of 443 mAh/g of $Cu_2CoSn_3S_8$. Consequently, although complete reversible capacity during the first cycle for $Cu_2CoSn_3S_8$ extends to a notorious value of ∼800 mAh/g, it is only partially preserved on prolonged cycling. The extended cycling behavior shown in Figure 10 reveals charge capacities close to 400 mAh/g up to cycle 10 for the tin compound. The titanium containing compositions have a more limited reversibility, which can be associated to the lack of the low voltage effect. These performances make the tin-containing spinel chalcogenide materials interesting candidates for anodes in lithium ion cells. To our knowledge no other spinel chalcogenide materials with relevant interest as a result of their potential electrochemical applications in lithium ion cells has been previously reported.

Concluding Remarks

Tin substitution by titanium is achieved in thiospinel compounds of general formula $Cu_2CoTi_xSn_{3-x}S_8$ within the complete range of x values. All phases can be described in the $Fd\bar{3}m$ space group with cobalt, tin, and titanium atoms randomly distributed in 16d sites with MS_6 octahedral coordination. A significant decrease in the cubic unit cell parameter of the spinel solids is observed on increasing the titanium content which cannot be explained on the basis of size effect alone. Instead, the effect of a larger covalent character of the bonds formed with sulfur atoms in the titanium-rich compositions should be taken into account. This phenomenon is revealed by the isomer shift values in the ^{119}Sn Mössbauer spectra.

The new solid−solution materials have been used as cathode material in lithium anode electrochemical cells. A first irreversible reduction step can be ascribed to a low-extension lithium insertion in the spinel structure with simultaneous reduction of $(Ti^{4+})_x(Sn^{4+})_{3-x}$. This process leads to the occurrence of Sn^0, as revealed by ^{119}Sn Mössbauer spectroscopy, together with a loss of long-range ordering in the solid products revealed by X-ray diffraction.

The extended discharge of the lithium cells leads to a good behavior in cycling experiments carried out in a low-voltage region. The admission of an enhanced amount of lithium−reversibly ∼400 mAh/g after extended cycling−is related to the occurrence of Sn^0 and takes place in a similar way to that previously described in tin oxides and oxosalts. The observed performances make these materials new interesting candidates for the anode in lithium ion cells.

Acknowledgment. The authors are indebted to the European Commission (Contract ERB-FMBI-CT98-3020), and the CNRS Program PICS505 for financial support.

CM990003E